Sveučilište u Zagrebu

PRIRODOSLOVNO-MATEMATIČKI FAKULTET

Chaiyaporn Lakmuang
Doctoral study in Chemistry, major: Physical Chemistry

# Energy Component Analysis for Electronically Excited States of Molecules: Why the Lowest Excited State Is Not Always the HOMO/ LUMO Transition

Chemistry seminar I

Based on
P. Kimber, F. Plasser, J. Chem. Theory Comput. 19 (2023) 2340–2352.

Zagreb 2026

# Contents

**Abstract**

Although the frontier-orbital energies and shapes are commonly used as a starting point in photoactive molecular design, this approach overlooks the inherently many-body nature of excited-state wavefunctions. This work highlights why excitation energies cannot only be considered from the orbital energy and introduces a physically meaningful framework for interpreting system behavior. The authors present two key parameters that directly contribute to the excited state energies: the Coulomb attraction and the repulsive exchange interaction. By analyzing the excited-state energy decomposition, the authors are able to explain the character of each state as well as the ordering of states in the model systems. In this work, two model examples are selected to demonstrate the utility of the tool they developed for energy component analysis and to clarify in which situations the lowest excited state in either the singlet or triplet state of the molecule does not originate from the HOMO/LUMO transition. The first model, the push-pull molecule ACRFLCN, illustrates that the lowest triplet state is a locally excited state that lies below the charge transfer HOMO/LUMO transition due to stabilization from the Coulomb attraction. The second model, naphthalene, is used to explain why the singlet HOMO/LUMO transition becomes the second excited state as a result of enhanced repulsive exchange interaction. Overall, this study offers a clear way to break down excitation energies into useful physical parts, supported by an easy-to-understand graphical approach, and applies it to clarify why the conventional molecular orbital (MO) picture can fail.

# 1 Introduction

Electron excitation reaction plays a crucial role in modern chemistry, for example, light-induced reactions in organic molecules [1, 2], semiconductors [3], and fluorescence [4]. A common practical strategy for modifying novel light-driven molecules begins with analyzing the frontier orbital energies, i.e., the energies of the highest occupied molecular orbital (HOMO) and lowest unoccupied molecular orbital (LUMO). Many research studies have proposed interesting approaches for manipulating these frontier orbital energies to achieve specific functional properties [5, 6, 7]. Although this HOMO-LUMO picture can offer a convenient starting point for qualitative reasoning, it often fails to capture the overall mechanism of the excited state. This limitation comes not only from neglecting contributions from other molecular orbitals but also from ignoring geometry relaxation processes [8, 9]. Moreover, different theoretical methods employ different algorithms to describe the orbital energy, making HOMO/LUMO energies heavily method dependent [10, 11]. Hence, a more physically based interpretation tool to decompose the excited energy into meaningful energy components, and also a method independent, will surely provide valuable insight and significantly improve our understanding of molecular photophysics and photochemistry.

The paper discussed in this essay proposed a logical framework that defines excitation energy components for excited state analysis developed from their previous publications [12, 13, 14]. This approach provides a clear physical interpretation of how excited energies can be decomposed into meaningful contributions and clarifies the limitations of the conventional MO picture. The authors present a set of correction terms that affect the excited energy beyond the HOMO/LUMO gap with a handy graphical representation. The first term, referred to as Coulomb attraction ($K_2$), stabilizes the energy gap between occupied and virtual orbitals due to attraction from the hole to the excited electron. The second term, exchange repulsion ($J_2$), describes the exchange interaction between an electron and a hole, which causes the singlet-triplet splitting. By evaluating these terms, the authors can easily point out when the lowest excited state (whether a singlet or a triplet state) of a molecule is not derived from the HOMO/LUMO transition.

To highlight these effects in real molecular systems, two candidate molecules with unique electronic properties are selected as model systems for the energy component analysis: the push-pull molecule ACRFLCN and the naphthalene molecule (Fig. 1). The ACRFLCN [15] is a bichromophoric molecule with a small singlet-triplet gap, making it an ideal case for studying the different energy components that determine the relative stability of locally excited (LE) and charge transfer (CT) states. The second molecule, naphthalene, serves as a typical aromatic molecule where the orbital energies of HOMO-1/HOMO and LUMO/LUMO+1 lie close together. It leads to several $\pi\pi^*$ excitations of similar energy with particular state character. The authors demonstrate how their approach can change this complex interaction into a simpler viewpoint, such as Platt's [16] and Pariser's [17] nomenclature.

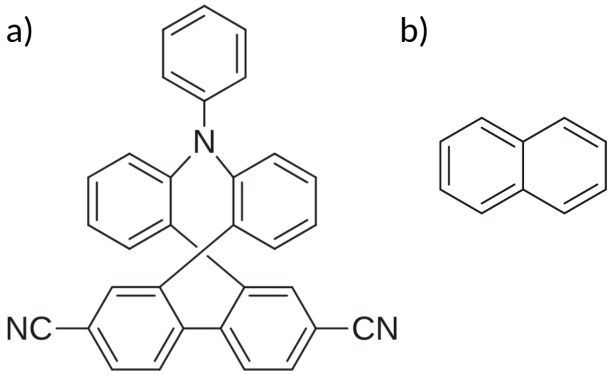


Figure 1: Molecular structures of (a) ACRFLCN and (b) naphthalene. Reproduced from ref. [18]

## 2 Theory and methods

This section summarizes the foundation of the authors' motivation for developing the energy decomposition approach, along with the practical framework for interpreting energy terms. Specifically, this section is organized into two major parts. The first part combines three subsections from the original paper: the theoretical background of excited-state energy decomposition, the interpretation of each energy term, and a detailed elaboration of how each energy term contributes to the overall excited-state energy based on TDDFT formalism. The second part, computational details, clarifies the computational methods used and introduces additional descriptors introduced by the authors to simplify the complex terms of the analysis.

### 2.1 Theoretical background and practical interpretation

The core idea of this approach arises from the two-orbital two-electron model (TOTEM) [14, 19, 20]. The first component is the energy required to promote an electron from the occupied orbital $\phi_i$ to the virtual orbital $\phi_a$, represented by the orbital energy gap $\epsilon_a - \epsilon_i$ (Fig 2a). For the triplet state transition, the electron spin is flipped when it is promoted from $\phi_i$ to $\phi_a$. The authors employ Koopmans' theorem to describe this transition by separately estimating the removal of an electron from $\phi_i$ (ionization energy) and reattachment of an electron to $\phi_a$ (electron affinity). The removal energy can be determined as

$$\epsilon_i = h_i + (ii|ii) \tag{1}$$

where $h_i$ is energy from the one-electron term, and $(ii|ii)$ is Coulomb repulsion between the two electrons occupying the same orbital $\phi_i$. To reattach an electron to $\phi_a$, the Koopmans theorem is applied again to estimate the electron affinity.

$$\epsilon_a^+ = h_a + (ii|aa) - (ia|ia) = \epsilon_a - (ii|aa) \tag{2}$$

Hence, the total excitation energy for the triplet state becomes

$$\Delta E_T = \epsilon_a^+ - \epsilon_i = \epsilon_a - \epsilon_i - \underbrace{(ii|aa)}_{K_2} \tag{3}$$

This expression shows that total energy is stabilized by the Coulomb attraction $(ii|aa)$ between occupied and virtual orbitals. The authors denote this term as $K_2$ and interpret it in the way that the excited electron is attracted by the hole it left in the ground state density (Fig.2b). Another important term can be derived only from the singlet excited state energy, which is expressed as

$$\Delta E_S = \epsilon_a - \epsilon_i - \underbrace{(ii|aa)}_{K_2} + \underbrace{2(ia|ia)}_{J_2} \tag{4}$$

The additional term "$2(ia|ia)$", denoted as $J_2$, comes from the electron-hole exchange interaction. This term appears because the singlet state must have an antisymmetric spin configuration, as required by the Pauli exclusion principle.

In fact, most of the excited-state quantum chemistry methods already include the term described above in their calculation. For example, in TDA-TDDFT, the excitation energies can be expressed as

$$\Delta E = \underbrace{\sum_{ia} |C_{ia}|^2(\epsilon_a - \epsilon_i)}_{h'} + J_2 + K_2 + XC_2 \tag{5}$$

The first term,$h'$, represents the single electron contribution derived from the ground-state Fock matrix. The final term, $XC_2$, accounts for additional exchange–correlation effects. Specifically for TDDFT, this term is the response of the exchange-correlation potential.

From eq. 5, it clearly illustrates why the excitation energy cannot be described solely by the energy difference between electron affinity and ionization potential, and which other terms can affect the total energy.

Another point worth mentioning from this paper is that orbital energies are heavily dependent on the computational method, whether from Hartree-Fock (HF) or DFT formalism. For HF, the HOMO/LUMO gap estimate via Koopmans' theorem provides only a rough approximation and often yields an inaccurate estimate of the excitation energy. However, for local functional or moderate exchange global hybrid functional (e.g., B3LYP, PBE0), both orbitals experience the same Kohn-Sham potential, making the HOMO/LUMO gap a reasonable first guess for excited energy. For this reason, the authors selected TDDFT with an optimally tuned range-separated density functional in their study for the energy decomposition analysis of excited states.

Within TDDFT/TDA and CIS, the $J_2$ term can be expressed in terms of one-electron transition density matrix (1-TDM) as the transition density of the electron-hole pair:

$$J_2 = \iint \frac{\rho_t(r_1)\rho_t(r_2)}{r_{12}} dr_1 dr_2 = \langle \rho_t | \hat{V} | \rho_t \rangle \tag{6}$$

where $r_{12}$ is the interelectronic separation. Physically, the $J_2$ represent the interaction of the transition density $(\rho_t)$ with it own electrostatic potential $(\hat{V}\rho_t)$ (Fig. 2c).

The $K_2$ term can be slightly affected by the function used in the range separation $s(r_{12})$. Using 1-TDM, the $K_2$ term can be written in simple form when correlation is neglected, and the two-body function $(\gamma_t)$ can be factorized into a single pair of natural transition orbitals (NTOs):

$$K_2 \approx -\iint \rho_h(r_h)\rho_e(r_e) \frac{s(r_{he})}{r_{he}} dr_h dr_e \tag{7}$$

Where $\rho_h$ and $\rho_e$ are hole and electron density, respectively. From this expression, the $K_2$ term can be represented as the interaction between the electron and hole densities, similar to the electrostatic representation in Eq. 6.

For the last term $XC_2$ in TDDFT/TDA, it represents the response of the exchange-correlation potential. It simply accounts for contribution terms to the excited energy that are not included in the orbital gap, Coulomb attraction $(K_2)$, and exchange repulsion $(J_2)$. According to the authors' results, this term is relatively small (less than 0.7 eV) and has only a minor effect on the overall excitation energy.

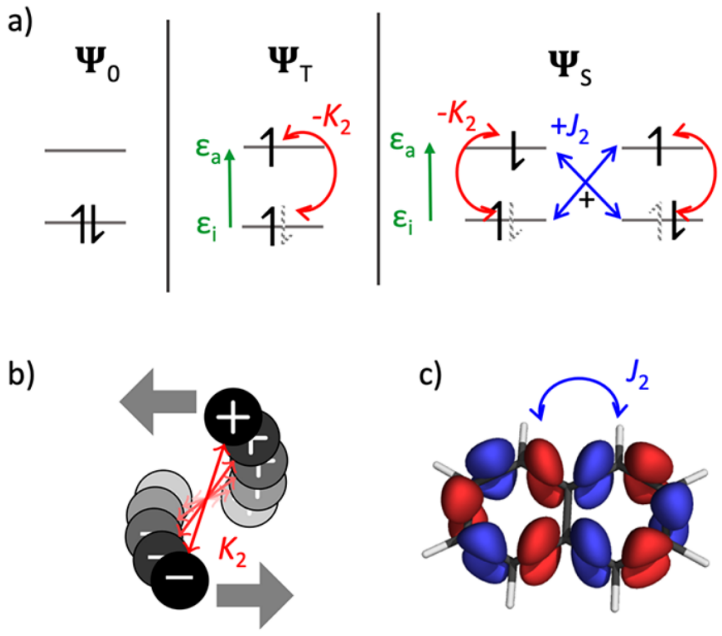


Figure 2: Representation of energy terms contributing to excited-state energies (a) excitation energies of triplet $(\Psi_T)$ and singlet $(\Psi_S)$; (b) the $K_2$ interpreted as a dynamic electron-hole binding energy, and (c) the $J_2$ corresponding to the transition density repulsion [18].

Moreover, the authors introduce two additional descriptors for analyzing the state character. The first descriptor, $d_{exc}$, provides a flexible measure of charge-transfer behavior, exciton binding, and Rydberg character. It is defined as a root-mean-square separation between electron

and hole. Due to the mathematical form similarity between $d_{exc}$ and $K_2$, the authors will point out their relationship in the discussion section.

The second one is the LOC descriptor, which measures the probability that an electron and a hole are located on the same basis function simultaneously. LOC is equivalent to 1 - CT when each basis function is treated as an individual fragment. States with LOC = 0.000 correspond to "-" states in Pariser's nomenclature, whereas values of LOC greater than 0.03 indicate "+" states.

### 2.2 Computational details

The geometries of ACRFLCN and napthalene are optimized using LRC-$\omega$PBEh/def2-SV(P) with response coefficient ($C_{HF}$) = 0.20 and range-separation parameter ($\omega$) = 0.2000 au and no influence of solvent. Then, the vertical excitations for both molecules are computed at the same level of theory with optimally tuned values of $\omega = 0.140$ au for ACRFLCN and $\omega = 0.225$ au for naphthalene. $h'$,$K_2$, $J_2$, and $XC_2$ were analyzed for each molecule as describe above.

Geometry optimizations and vertical excitation calculations were carried out using Q-Chem versions 5.2 and 6.0. The author also utilize The libwfa library in Q-Chem to analyze wave functions, ESPs, and to compute the LOC descriptor. To decompose the excited-state energy into each component ($h'$, $K_2$, $J_2$, and $XC_2$), the keyword "EXCIT_ENERGY_COMPONENTS = TRUE" was specified in the Q-Chem input files. General post-processing of excited-state results was performed using TheoDORE, while ESP visualizations were generated with PyMOL.

## 3 Results and discussion

As discussed in Section 2.1, the first term in equation 5 approximately corresponds to the minimum HOMO/LUMO transition, whereas the remaining three terms play an important role in adjusting the excitation energy depending on the nature of the excited state, particularly for locally excited (LE) states. In the triplet state, the $K_2$ term makes the dominant contribution to the energy shift. The state with a larger $K_2$ will be lower in energy and lie below other states. While in the singlet state, the contribution of the $J_2$ term can be more important and may raise the energy above that of another singlet excited state. Overall, the post-MO terms are particularly important for LE states where triplet LE states are stabilized via $K_2$ and singlet LE states are destabilized via $J_2$. The authors selected ACRFLCN and napthalene molecules to exemplify these two cases.

### 3.1 ACRFLCN: effect of CT and LE states

ACRFLCN is a bichromophoric molecule that contains an acridine donor (upper part) and a triphenylamine acceptor (lower part). Both fragments are linked by a spiro junction, making them perpendicular to each other. Computational results show that HOMO is located on the

donor part, while the LUMO and HOMO-1 are primarily located on the acceptor part. As a result, the HOMO/LUMO transition can be identified as an intramolecular CT state, whereas the HOMO-1/LUMO transition is classified as an LE state.

Using TDDFT with the Tamm–Dancoff approximation, the authors calculated the HOMO to LUMO and HOMO–1 to LUMO gaps to be 5.856 eV and 6.933 eV, respectively. However, they found that the lowest excited state ($T_1$) is located at 3.030 eV, which is mainly due to the HOMO-1 to LUMO transition, forming a locally excited state. The next triplet state $T_2$ is found at 3.324 eV, which is purely a HOMO/LUMO transition and corresponds to a CT state. The first singlet state lies only 0.012 eV above the $T_2$ state and has the same electron configuration as the $T_2$ state. Finally, the bright $S_2$ state occurs at 4.258 eV, which is a locally excited state dominated by the HOMO-1 to LUMO transition. All four excited-state properties are summarized in Table 1. The authors point out that the lowest excited state of each multiplicity ($T_1$ and $S_1$) has a different character, and the energy gap between locally excited states (1.228 eV) is much larger than that between CT states (0.012 eV).

Table 1: Excitation energies (eV), oscillator strengths (f), and main electronic configurations of the first two singlet and triplet states of ACRFLCN using LRC-$\omega$PBEh/def2-SV(P) (TDA). Reproduced from ref. [18]

| State | ΔE | f | [a]Configurations |
|---|---|---|---|
| $^3$LE ($T_1$) | 3.03 | - | $0.85h_1l + 0.37h_3l$ |
| $^3$CT ($T_2$) | 3.324 | - | $0.99hl$ |
| $^1$CT ($S_1$) | 3.336 | 0.000 | $0.99hl$ |
| $^1$LE ($S_2$) | 4.258 | 0.334 | $0.91h_1l$ |

[a] Dominant configurations and coefficients; $h_xl_y$ refers to the HOMO–$x$/LUMO+$y$ transition.

The energy component analysis was used to explain these findings. The authors plotted each component in a stacked bar graph, with the positive contributions ($h'$ and $J_2$) stacked on top of each other and the negative contributions ($K_2$ and $XC_2$) treated as offset, as shown in Figure 3. Note that $XC_2$ values in LRC-$\omega$PBEh level are always negative, although this may vary depending on the functional used. From this graph, the total excitation energy can be read at the top of the left bar for each state. In triplet states, the $h'$ term (green) of $^3$LE state is 7.960 eV, which is larger than $^3$CT state (6.041 eV). However, $^3$LE is massively stabilized by $K_2$ (red) and some $XC_2$ (yellow), causing it to be in the lowest state. The bottom graph illustrates the exciton size, showing that the $^3$LE state has a $d_{exc}$ below 4.0 Å, whereas $^3$CT exceeds 5.5 Å. This highlights an inverse correlation between the $K_2$ and $d_{exc}$ values. When comparing $^3$CT and $^1$CT, their energy contribution and exciton size are nearly identical. The exchange repulsion in these states vanishes due to the complete charge separation character. For the $^1$LE state, the state character differs significantly from its triplet counterpart ($^3$LE), has a higher exciton size (4.539 Å) and a smaller $K_2$ term (-3.479 eV). The energy gap between $^3$LE and $^1$LE is 1.228

eV, primarily coming from +0.426 eV from $J_2$ and + 0.725 eV from $\Delta K_2$. Furthermore, the authors also compute the formal $J_2$ term for the singlet state using the same response vector as the $^3$LE state, but with reversed spin coupling, to examine the similarity of their wave functions. Remarkably, the formal $J_2$ was found to be 2.784 eV, which would place the excitation energy of the corresponding singlet state at 5.814 eV. This result suggests that the $^1$LE state modified its wave function compared to $^3$LE to lower its energy by reducing the exchange repulsion from 2.784 eV to 0.426 eV. This stabilization is achieved by allowing the singlet HOMO/LUMO configuration to interact more strongly with other electronic configurations.

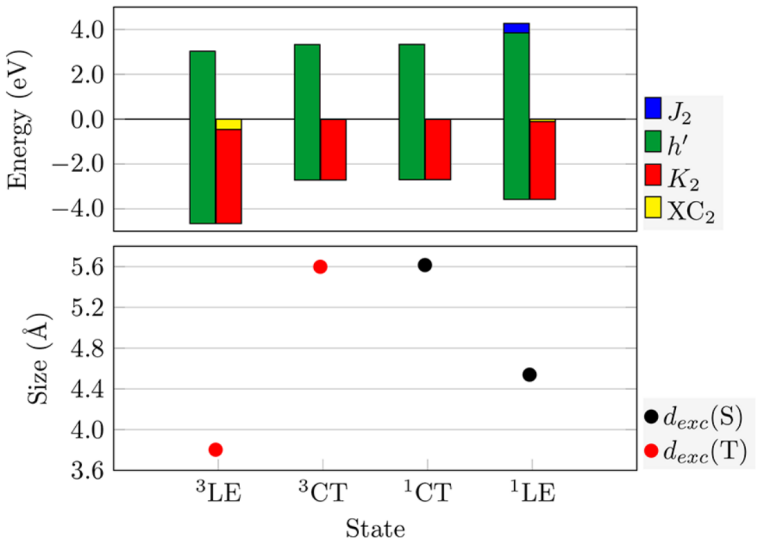


Figure 3: Energy components (top) and exciton size descriptors (bottom) for the excited states of ACRFLCN. Exciton sizes $d_{exc}$ are displayed in black for singlets and red for triplets. [18].

Figure 4 provides a visual representation of the two-electron contribution. The hole and electron natural transition orbitals (NTOs), shown in cyan and orange, are displayed at the center. The corresponding electron (blue) and hole (red) densities, along with their electrostatic potentials (ESPs) associated with the $K_2$ term, are shown above. Transition densities and their ESPs responsible for the $J_2$ contribution are shown in the lower panel.

The hole ($\rho_h$) and electron ($\rho_e$) densities are constructed by weighted sums over the NTOs, along with their associated ESPs. As shown in the top panel of Figure 4, the electron density and its ESP exhibit very similar shapes for all states and are primarily localized on the acceptor group. In contrast, the hole density reflects the nature of the excited state: for charge-transfer (CT) states, it is localized on the donor group, whereas for locally excited (LE) states, it remains on the acceptor group. The $K_2$ term can be approximated by computing the overlap between the hole density and the electron ESP or vice versa. In CT states, the $K_2$ values are greatly reduced due to a very small overlap between hole density and electron ESP.

The bottom part illustrates that the product of hole and electron NTOs leads to the transition density for the excited state and its associated ESPs. The $J_2$ term is obtained by self-repulsion of the transition density (eq. 6). In CT states, the transition density and its ESP are very small,

leading to a correspondingly small $J_2$ term. In contrast, the $^1$LE state exhibits a moderate transition density, which generates a strong ESP with a clear dipolar shape, explaining the stronger $J_2$ term. The authors also highlight a key difference in the wave functions between the $^1$LE ($S_2$) and $^3$LE ($T_1$) states, which are mainly composed of the HOMO-1/LUMO transition. A clear difference in hole NTO shape can be observed: in the $T_1$ state, it is entirely located on the acceptor part (Figure 4 (a)), whereas the spatial distribution extends partially into the donor unit in $S_2$ (Figure 4 (d)). This change leads to enhanced charge transfer, which can be seen in the larger $d_{exc}$ value of $S_2$ compared to $T_1$ in Figure 3. This leads to reduced electron–hole overlap, resulting in diminished transition density and ESPs, and consequently a reduction in both the $K_2$ and $J_2$ terms.

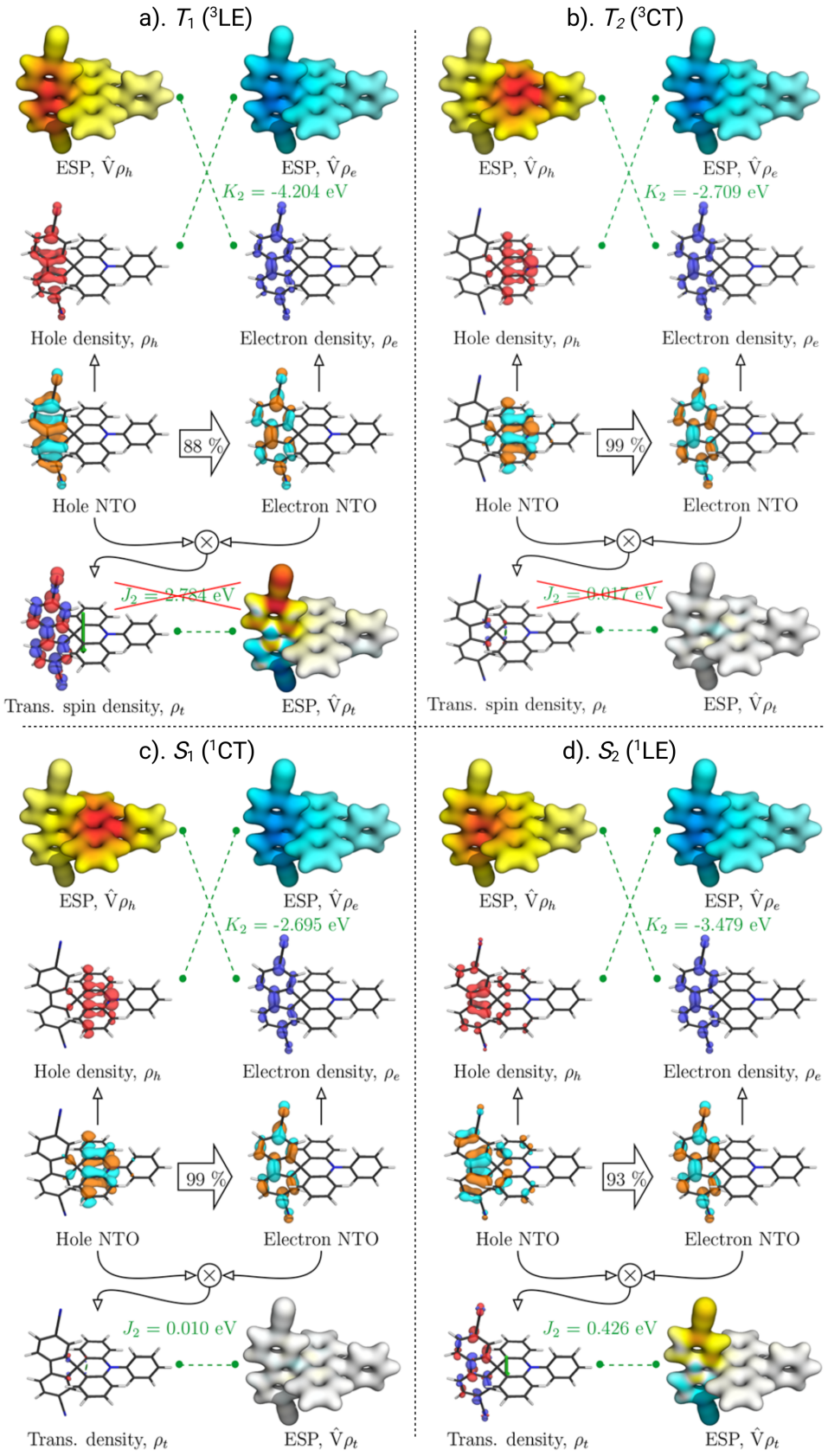


Figure 4: Energy contribution analysis for the (a) $T_1$ ($^3$LE), (b) $T_2$ ($^3$CT), (c) $S_1$ ($^1$CT), and (d) $S_2$ ($^1$LE) states of ACRFLCN. Electron and hole densities and their induced ESPs are shown at the top, followed by the dominant NTOs in the middle, and the transition density with its ESP at the bottom. Modified from ref. [18].

### 3.2 Naphthalene: Ionic and Covalent States

Napthalene is a classic model of an aromatic molecule, which all excited states can be constructed from the same set of MOs. As a result, considering only the MO energy gap is insufficient to distinguish between different excited state characters. In this case, the alternative frameworks, such as Platt's nomenclature and Pariser's +/- nomenclature, can be used to provide valuable insight. Another important aspect of this system is that the relative signs of the interacting configurations also play a crucial role in determining the excited state energies.

The first four singlet and triplet excited states of napthalene, along with their properties, were calculated and reported in Table 2. All of these states can be explained by the transition from the HOMO-1 and HOMO to the LUMO and LUMO+1. The HOMO/LUMO and HOMO-1/LUMO+1 transitions are dominant and do not mix with each other, giving $1B_{2u}^{+}$ and $1B_{2u}^{-}$ state characters as shown in Figure 5. On the other hand, the transition of HOMO-1/LUMO and HOMO/LUMO+1 are greatly mixed, forming the $1B_{3u}^{+}$ and $1B_{3u}^{-}$ states, which differ only in the relative sign used in their linear combination, as introduced by Pariser [17]. In Table 2, the LOC descriptor serves as a convenient parameter for distinguishing between "+" and "-" states, which becomes zero for "-" state. Notably, the excited states span an energy range of almost 4 eV, even though they are built from the same four MOs. To gain further insight into this energy ordering, the authors analyzed the individual energy contributions using energy component analysis presented in Figure 6.

Table 2: Excitation energies (eV), oscillator strengths (f), main configurations, and LOC values of the first four triplet and singlet states of Napthalene using LRC-$\omega$PBEh/def2-SV(P) (TDA). Reproduced from ref. [18]

| State | $\Delta$E | f | [a]Configurations | LOC |
|---|---|---|---|---|
| $1^3B_{2u}^{+}$ ($T_1$) | 3.071 | - | 0.93$hl$ | 0.138 |
| $1^3B_{3u}^{+}$ ($T_2$) | 4.212 | - | 0.74$h_1l$ + 0.64$hl_1$ | 0.063 |
| $1^3B_{3u}^{-}$ ($T_3$) | 4.510 | - | 0.74$hl_1$ - 0.65$h_1l$ | 0.000 |
| $2^3B_{2u}^{+}$ ($T_4$) | 4.684 | - | 0.95$h_1l_1$ | 0.088 |
| $1^1B_{3u}^{-}$ ($S_1$) | 4.779 | 0.000 | 0.70$hl_1$ - 0.70$h_1l$ | 0.000 |
| $1^1B_{2u}^{+}$ ($S_2$) | 5.085 | 0.097 | 0.93$hl$ | 0.074 |
| $1^1B_{3u}^{+}$ ($S_3$) | 6.815 | 2.023 | 0.68$h_1l$ + 0.68$hl_1$ | 0.040 |
| $2^1B_{2u}^{+}$ ($S_4$) | 6.990 | 0.393 | 0.89$h_1l_1$ | 0.072 |

[a] Dominant configurations and coefficients; $h_xl_y$ refers to the HOMO–$x$/LUMO+$y$ transition.

In napthalene, all excited states can be considered locally excited ,as confirmed by their low exciton size ($d_{exc} < 3.5$ Å). Thus, the $K_2$ values are quite similar for all excited states, around -5 eV. When comparing $T_1$ and $T_2$, the energy gap is 1.141 eV, where only 0.413 eV comes from $\Delta h'$. The main contributions arise from $\Delta K_2$ = 0.414 eV and $\Delta XC_2$ = 0.313

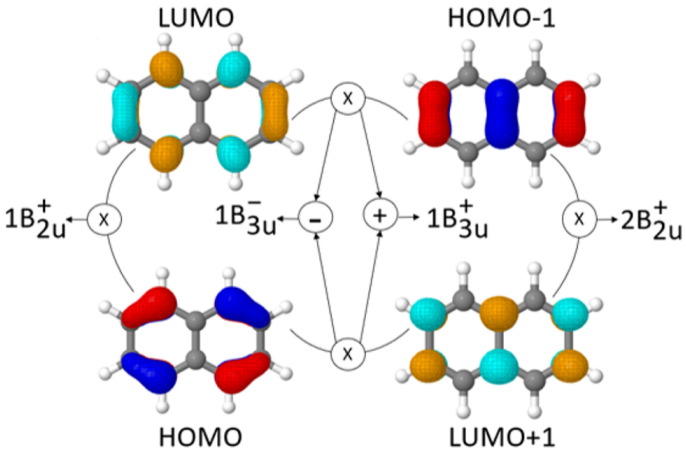


Figure 5: Linear combinations of canonical orbitals of lowest four triplet and singlet excited states of napthalene. [18].

eV, indicating that $T_1$ is more localized than $T_2$. The next pair, $T_2$ and $T_3$, differs only in the sign of their state character,but they are separated by around 0.3 eV. This difference originates from $\Delta K_2$ = 0.209 eV and $\Delta XC_2$ = 0.178 eV, which are enhanced for the more local nature of $1^3B^{+}_{3u}$ state, as reflected by its higher LOC value. Next, the $T_4$ state is located above $T_3$ state because its involved the HOMO-1/LUMO+1 transition, which has a larger energy gap, leading to an enhanced $\Delta h'$ = 0.816 eV. However, $T_4$ also exhibits more local nature than $T_3$, making the larger offset part contribution from $\Delta K_2$ and $\Delta XC_2$.

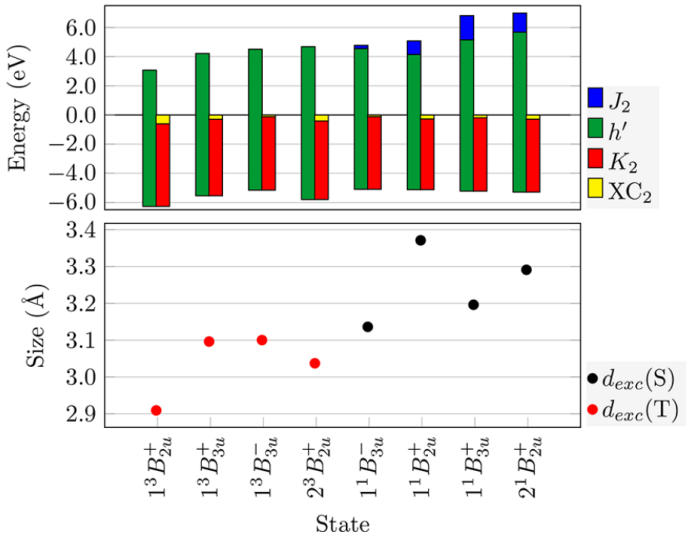


Figure 6: Energy components (top) and exciton size descriptors (bottom) for the excited states of napthalene. Exciton sizes $d_{exc}$ are displayed in black for singlets and red for triplets. [18].

The first singlet excited state, $S_1$, has the same state character as $T_3$, stressing the different role of the $J_2$ term in singlet and triplet states, with $J_2$ = 0.234 eV in this case. The $S_2$, dominated by HOMO/LUMO transition, appears as the sixth excited state despite its low one-electron component ($h'$ = 9.270 eV) because its energy is strongly destabilized by exchange

repulsion ($J_2$ = 0.939 eV). The authors also computed the formal $J_2$ using the same response vector as $T_1$ and obtained 4.203 eV. As in the ACRFLCN case, this indicates that the exchange term is strongly reduced when going from the triplet to the singlet by promoting the CT character with the cost of reduced $K_2$ and $XC_2$. The $S_3$ state is dominated by the HOMO-1/LUMO and HOMO/LUMO+1 transition, causing a large $h'$ term. In addition, a relatively large $J_2$ contribution (1.672 eV) further pushes this state to the higher excitation energy. Finally, the $S_4$ has a high one-electron term (10.971 eV) due to the HOMO-1/LUMO+1 transition, along with a high $J_2$ term (1.313 eV), placing it at the highest energy among all states.

# 4 Conclusion

This work proposes an energy component analysis for excited states, which provides a valuable framework for investigating and explaining the excited state order and highlighting the fact that relying on only the MO gap is insufficient to describe the real systems. The excited state energies can be decomposed into mainly four parts: the weighted orbital energy difference ($h'$), a Coulomb attraction ($K_2$), an exchange repulsion ($J_2$), and two-electron exchange/correlation ($XC_2$). In locally excited state, the $K_2$ term is enhanced, leading to a significant stabilization, especially for the triplet states. In contrast, the $J_2$ is also be promoted and tends to destabilize the locally excited singlet state.

For example, in ACRFLCN, the HOMO/LUMO transition forms the $T_2$ state, while HOMO-1/LUMO transition is represented by the lowest $T_1$ state. This order can be explained by the fact that $T_1$ has a locally excited state with enhanced $K_2$, causing the overall energy to be lower than $T_2$, despite its larger MO gap. In the singlet state, the order was reversed because of the enhanced $J_2$ term in the locally excited state.

In the case of napthalene, where all excited states can be considered locally excited, the HOMO/LUMO transition corresponds to the $T_1$, whereas the lowest singlet state, $S_1$, is constructed by the linear combination between HOMO-1/LUMO and HOMO/LUMO+1 transition. Overall, all eight excited states were found to be described by linear combinations of transitions involving only four canonical orbitals: HOMO-1, HOMO, LUMO, and LUMO+1.

## References


[1] Ziping Li, Yongfeng Zhi, Pengpeng Shao, Hong Xia, Guosheng Li, Xiao Feng, Xiong Chen, Zhan Shi, and Xiaoming Liu. Covalent organic framework as an efficient, metal-free, heterogeneous photocatalyst for organic transformations under visible light. *Applied Catalysis B: Environmental*, 245:334–342, 2019.

[2] Paolo Costa, Alberto Vega-Penaloza, Leonardo Cognigni, and Marcella Bonchio. Light-induced organic transformations by covalent organic frameworks as reticular platforms for selective photosynthesis. *ACS Sustainable Chemistry & Engineering*, 9(47):15694–15721, 2021.

[3] X-Y Zhu, Q Yang, and M Muntwiler. Charge-transfer excitons at organic semiconductor surfaces and interfaces. *Accounts of chemical research*, 42(11):1779–1787, 2009.

[4] Ryutaro Komatsu, Tatsuya Ohsawa, Hisahiro Sasabe, Kohei Nakao, Yuya Hayasaka, and Junji Kido. Manipulating the electronic excited state energies of pyrimidine-based thermally activated delayed fluorescence emitters to realize efficient deep-blue emission. *ACS Applied Materials & Interfaces*, 9(5):4742–4749, 2017.

[5] Kazuo Tanaka. New strategy for lowering the energy levels of one frontier molecular orbital in conjugated molecules and polymers based on aza-substitution at the isolated homo or lumo. *Polymer Journal*, 56(2):61–70, 2024.

[6] Masayuki Gon and Kazuo Tanaka. Utilization of hypervalent bonds as a novel strategy for manipulating energy levels of $\pi$-conjugated systems. *European Journal of Organic Chemistry*, 27(45):e202400738, 2024.

[7] Shunichiro Ito, Masayuki Gon, and Kazuo Tanaka. Effects of heavy p-block elements on photophysical properties of $\pi$-conjugated complexes and organoelement compounds. *European Journal of Inorganic Chemistry*, 27(21):e202400180, 2024.

[8] Jean-Luc Brédas. Organic electronics: does a plot of the homo–lumo wave functions provide useful information?, 2017.

[9] Jeffrey Roshan De Lile, Sung Gu Kang, Young-A Son, and Seung Geol Lee. Do homo–lumo energy levels and band gaps provide sufficient understanding of dye-sensitizer activity trends for water purification? *ACS omega*, 5(25):15052–15062, 2020.

[10] Andreas Dreuw and Martin Head-Gordon. Single-reference ab initio methods for the calculation of excited states of large molecules. *Chemical reviews*, 105(11):4009–4037, 2005.

[11] R Van Meer, OV Gritsenko, and EJ Baerends. Physical meaning of virtual kohn–sham orbitals and orbital energies: an ideal basis for the description of molecular excitations. *Journal of chemical theory and computation*, 10(10):4432–4441, 2014.

[12] Zheng Pei, Qi Ou, Yuezhi Mao, Junjie Yang, Aurelien de la Lande, Felix Plasser, Wanzhen Liang, Zhigang Shuai, and Yihan Shao. Elucidating the electronic structure of a delayed fluorescence emitter via orbital interactions, excitation energy components, charge-transfer numbers, and vibrational reorganization energies. *The journal of physical chemistry letters*, 12(11):2712–2720, 2021.

[13] Zheng Pei, Junjie Yang, Jingheng Deng, Yuezhi Mao, Qin Wu, Zhibo Yang, Bin Wang, Christine M Aikens, Wanzhen Liang, and Yihan Shao. Analysis and visualization of energy densities. ii. insights from linear-response time-dependent density functional theory calculations. *Physical Chemistry Chemical Physics*, 22(46):26852–26864, 2020.

[14] Patrick Kimber and Felix Plasser. Toward an understanding of electronic excitation energies beyond the molecular orbital picture. *Physical Chemistry Chemical Physics*, 22(11):6058–6080, 2020.

[15] Gábor Méhes, Hiroko Nomura, Qisheng Zhang, Tetsuya Nakagawa, and Chihaya Adachi. Enhanced electroluminescence efficiency in a spiro-acridine derivative through thermally activated delayed fluorescence. *Angewandte Chemie (International ed. in English)*, 51(45):11311–11315, 2012.

[16] John R Platt. Classification of spectra of cata-condensed hydrocarbons. *The Journal of chemical physics*, 17(5):484–495, 1949.

[17] Rudolph Pariser. Theory of the electronic spectra and structure of the polyacenes and of alternant hydrocarbons. *The Journal of Chemical Physics*, 24(2):250–268, 1956.

[18] Patrick Kimber and Felix Plasser. Energy component analysis for electronically excited states of molecules: why the lowest excited state is not always the homo/lumo transition. *Journal of Chemical Theory and Computation*, 19(8):2340–2352, 2023.

[19] Mark E Casida and Miquel Huix-Rotllant. Progress in time-dependent density-functional theory. *Annual review of physical chemistry*, 63(1):287–323, 2012.

[20] Xian-Kai Chen, Dongwook Kim, and Jean-Luc Brédas. Thermally activated delayed fluorescence (tadf) path toward efficient electroluminescence in purely organic materials: molecular level insight. *Accounts of Chemical Research*, 51(9):2215–2224, 2018.